Composites Part C: Open Access 6 (2021) 100183

Contents lists available at ScienceDirect

Composites Part C: Open Access

journal homepage: www.sciencedirect.com/journal/composites-part-c-open-access

Monte Carlo strategy for SEM-EDS micro-nanoanalysis of geopolymer composites

Daniele Moro, Gianfranco Ulian, Giovanni Valdrè *

Centro di Ricerca Interdisciplinare di Biomineralogia, Cristallografia e Biomateriali, Dipartimento di Scienze Biologiche, Geologiche e Ambientali, Università di Bologna "Alma Mater Studiorum", Piazza P. San Donato 1, 40126 Bologna, Italy

ARTICLE INFO

Keywords:
Nanocomposites
Geopolymers
Monte Carlo method
SEM-EDS X-ray nanoanalysis

ABSTRACT

The development, optimization and application of new geopolymer composite materials must necessarily go through a precise and accurate physico-chemical and mineralogical characterization down to the micro and nanoscale. In this regard, SEM-EDS X-ray microanalysis is widely and successfully employed by the scientific community and industry. However, the nano-to-micrometre sized architecture of many geopolymer composites introduces many difficulties and issues in SEM-EDS quantification, with potential large sources of error that should carefully be taken into account and investigated. In this work, a SEM-EDS Monte Carlo approach is proposed to study the complex physical phenomena at the basis of the quantification issues and errors, through the investigation of: (i) a not completely reacted sodium-poly(sialate-siloxo) geopolymer, and (ii) a geopolymer composite with a potassium-poly(sialate-siloxo) matrix and basalt-derived glass fibres reinforcement. The Monte Carlo simulation evinced a strong influence of the nano-microsized specimen architecture (e.g., basalt fibre size and shape, different elemental composition between fibre and matrix) on the measured X-ray intensity, with contributions also depending on the SEM electron beam energy. The proposed approach provided fundamental indications for selecting optimal operative conditions depending on the type of geopolymer sample, shape, size with the specific SEM-EDS setup and silicon drift EDS detector here used.

Introduction

Geopolymers are inorganic ceramic-like materials introduced by Davidovits in 1979 [1]. Their polymeric character is due to the formation of molecular units linked in chains or networks by covalent bonds [2]. The typical starting raw materials are rock-forming minerals, amorphous silica, industrial by-products, whose mineralogical and crystallo-chemical properties are fundamental key factors [2–4]. For instance, the use of dehydroxylated kaolinite, known as metakaolin, in an alkaline synthesis route with (Na,K)-hydroxides and/or soluble alkali-silicates gives a (Na,K)-poly(sialate-soloxo) geopolymer, in a 3D-framework of SiO_4 and AlO_4 tetrahedra [2]. The micro/nano-structure of geopolymers that depends on a variety of factors, such as lability of silicate species, were observed to be characterized by nanoclusters even down to 5 nm in size [2,5–7]. Hence, their characterization requires advanced microscopy and micro-nanoanalytical techniques already successfully applied in mineralogical sciences and related fields, such as transmission electron microscopy (TEM), electron energy loss spectroscopy (EELS), scanning electron microscopy (SEM) together with energy dispersive X-ray microanalysis (EDS), nuclear magnetic resonance (NMR) and scanning probe microscopy [5,8–11]. Geopolymers are attracting the interest of the scientific community and industry due the potential high performance and lower environmental impact with respect to ordinary Portland cement [12,13]. Furthermore, new composite materials are recently investigated based on the combination of geopolymers and inorganic or natural fibres, with the aim to enhance strength and fracture toughness. The development of fibre-reinforced geopolymer composites for structural applications mostly employs carbon, basalt-derived or glass fibres, with the recent study of the application also of alumina, silicon carbide and mullite [12,14–16].

Among the above mentioned characterization techniques, scanning electron microscopy (SEM) together with energy dispersive X-ray microanalysis (EDS) is a widely used methodology for the study of several fundamental properties of the newly synthesized geopolymeric composites as prepared and after mechanical stress application (e.g., micro-to-nano morphology, chemistry and structure of both the particle/fibre reinforcement and geopolymer matrix), because of the ease of

* Corresponding author.
E-mail address: giovanni.valdre@unibo.it (G. Valdrè).

https://doi.org/10.1016/j.jcomc.2021.100183
Received 10 August 2021; Accepted 11 August 2021
Available online 13 August 2021

application and useful morphological and micro-chemical information provided [17,18]. This type of investigation can provide fundamental contributions both on the efficiency of the geopolymeric reaction in terms of homogeneity of the geopolymer matrix and complete consumption of reagents, and on the preservation or corrosion of the micro/nano-particles/fibres, their distribution in the matrix, and also analysis of particle/fibre – matrix interface. All these characteristics of the geopolymer composite deeply influence the mechanical behaviour of the final composite product.

However, in the SEM-EDS analysis, the micro-to-nano architecture of geopolymer composites determines several issues that make it often not possible to assume the hypothesis of application of the corrections for matrix effects (*e.g.,* ZAF procedures), since the specimen is neither "infinitely" thick, nor flat [19]. In fact, the qualitative and quantitative chemical analysis of micro and even nano-domains (e.g., inhomogeneities, reaction products, inclusions, particles, fibres) is often a challenge since several factors may affect the measurement and lead to incorrect interpretations. As already cited, these factors are: (1) the small particle/fibre thickness compared to the electron beam penetration depth; (2) the inelastic and elastic electron scattering inside the micro/nano-particle/fibre, strongly dependent on the average atomic number; (3) the path of absorption of X-rays toward the detector, together with the take-off angle and the contribution of secondary fluorescence, whose volume of generation could be more than an order of magnitude greater than that of X-rays generated by electron impact [20]; and (4) the specimen-to-EDS detector configuration.

In this work, we present an approach based on SEM-EDS Monte Carlo simulations to investigate the physical phenomena at the base of the cited issues in the analysis of geopolymer composites. The Monte Carlo simulation allows to model the electron transport and generation of X-rays in solids under realistic experimental conditions [21–23], and was here used to predict systematic errors in SEM-EDS quantitative measurements of geopolymer micro/nano-composite structures and provide a suitable analytical strategies for a correct nano-analysis. Two cases were considered for this purpose:

- A not completely reacted sodium-poly(sialate-siloxo) geopolymer (Na-PSS);
- A geopolymer composite with a potassium-poly(sialate-siloxo) matrix (K-PSS) and basalt-derived glass fibres reinforcement.

Several SEM-EDS operating conditions were simulated to investigate their effect on the qualitative and quantitative nano-microanalysis and suggest a strategy for precise and accurate measurements.

Models in SEM-EDS Monte Carlo simulations

Physical models

The Monte Carlo method is a very effective tool to simulate the trajectory of electrons inside materials, also calculating the generation and transport of X-rays in complex samples, and towards realistic EDS detectors, and to simulate the EDS X-ray spectrum [22,23]. Indeed, geopolymer composites present complex architectures of the constituent materials which entail not obvious interactions with the energetic electrons of the SEM-EDS. It is therefore fundamental to achieve a complete understanding of the involved physical phenomena (i.e., electrons scattering, and generation, absorption and fluorescence of X-rays) for a precise and accurate quantitative SEM-EDS X-ray microanalysis of geopolymer composites and their micro-/nanosized substructures.

The SEM-EDS Monte Carlo model considers the 3D trajectories of electrons as sequences of straight segments, each weighted by the mean free path and ended by an elastic scattering event. The continuous slowing down approximation is here employed to take into account the average energy loss due to inelastic collisions [24]. A basic screened Rutherford model [25], the Mott scattering cross section of Czyzewski and co-workers [26], and the Mott cross section of Jablonski and co-workers [27] model the elastic scattering. The Joy-Luo expression [28], that is an empirical modification of Bethe energy loss equation [29], models the energy loss dE with respect to the travelled distance ds (keV/cm):

$$\frac{dE}{ds} = -7.85 \times 10^4 \frac{Z\rho}{AE_i} \ln\left(\frac{1.166E_i}{J^*}\right)$$

$$J^* = \frac{J}{1+(kJ/E)}$$

$$k = 0.731 + 0.0688\log_{10}Z$$

$$J = \left(9.76Z + 58.5Z^{-0.19}\right) \times 10^{-3}$$

where A is the atomic weight (g/mole), E_i the electron energy (keV) at any point in the specimen, Z the atomic number, ρ the density (g/cm^3), J the average loss in energy per event and J^* the modified mean ionization potential.

The parameterized analytical expression of Bote and Salvat is used to model the ionisation cross-section σ_i [30,31]:

$$for\ U \le 16,\ \sigma_i = 4\pi a_0^2 (U-1) \Big/ U^2 \left(a_1 + a_2 U + a_3/(1+U) + a_4/(1+U)^3 + a_5/(1+U)^5\right)^2$$

$$for\ U > 16,\ \sigma_i = U \Big/ (U+b) 4\pi a_0^2 A_i \Big/ \beta^2 \left\{ \left[\ln X^2 - \beta^2\right] \left(1 + g_1 X^{-1}\right) + g_2 + g_3 \left(1-\beta^2\right)^{1/4} + g_4 X^{-1} \right\}$$

where $U = E/E_c$ is the overvoltage of electrons with kinetic energy E for ionization of a particular shell with critical ionization energy E_c, a_0 is the Bohr radius, a_1, a_2, a_3, a_4, a_5, b, g_1, g_2, g_3, g_4 are parameters characteristic of each element and electron shell, $A_i = \alpha^2 M_j^2/2$ with α fine-structure constant and M_j^2 squared dipole-matrix element for ionization, $\beta = v/c$ with v electron velocity and c speed of light, $X \equiv p/(m_e c)$ with p electron momentum and m_e electron mass.

The fluorescence yields tabulated by Perkins and co-workers are employed to model the relaxation process of core-shell vacancies for the characteristic X-rays generation, in isotropic conditions and without considering photon polarization [32]. Seltzer and Berger's tabulated partial and total cross-sections for Bremsstrahlung production are used for primary continuum (Bremsstrahlung) not isotropic emission [33–36]. X-ray absorption considers the photoelectric component of the mass absorption coefficients calculated by Chantler and co-workers [37].

Both Bremsstrahlung and characteristic primary X-ray photons are propagated in a random direction and are absorbed by photoionization or escape the materials after a computed mean free path for photoionization. Following the specific probabilities, the relaxation, consequent upon photoionization, yields secondary X-ray fluorescence of the absorbing element [20].

A realistic SEM-EDS setup was modelled, considering a modern Silicon Drift Detector (SDD) and an electron probe of 5 nm. The SDD energy

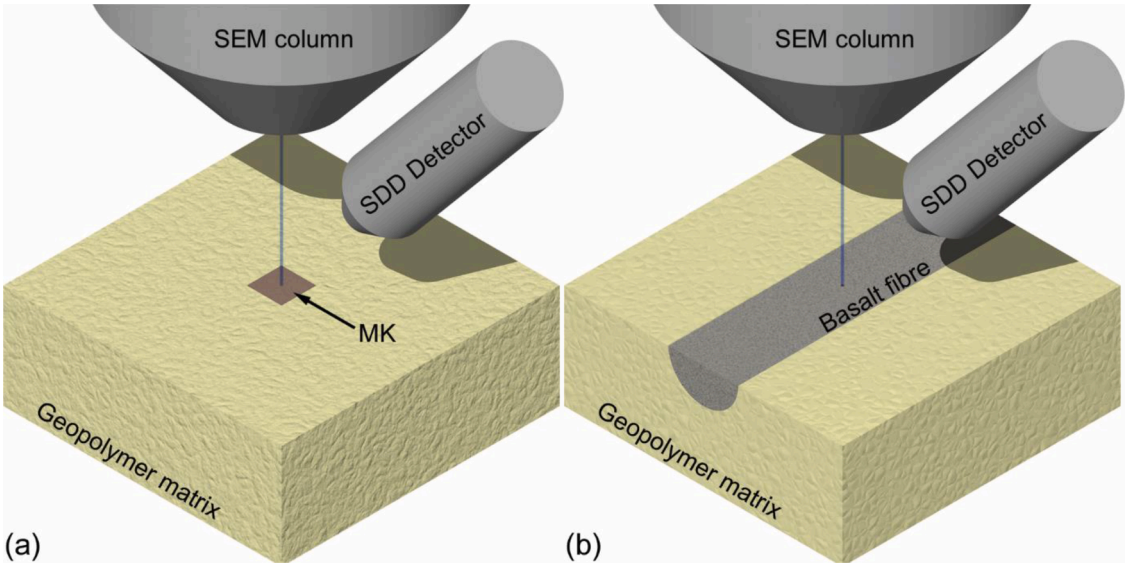

Fig. 1. Geometrical models of the simulated SEM-EDS set-up. (a) Metakaolin booklet, 2 μm x 2 μm wide and with a variable thickness down to 0.1 μm, embedded in a sodium-poly(sialate-siloxo) geopolymer, with the electron beam focussed on the centre of the top-surface of the particle. (b) Longitudinal section of a basalt-derived glass fibre embedded in a potassium-poly(sialate-siloxo) geopolymer matrix, with the long axis of the fibre oriented perpendicularly to the detector, and the electron beam focussed on the centre of the fibre top-surface. The silicon drift EDS detector was set with an elevation angle of 35° both in (a) and (b). Schematics were modelled with the POV-Ray software.

Table 1
Oxides mass fraction (weighted percentage) of basalt-derived glass fibre.

SiO_2	Al_2O_3	Fe_2O_3	CaO	MgO	Na_2O	K_2O	TiO_2	P_2O_5	MnO
50	15	14	9	6	2.3	1.7	1.6	0.2	0.2

dispersive X-ray detector was simulated taking into account its resolution and efficiency, with the following physical and technical parameters: an ultrathin polymer window (Moxtek AP 3.3 film), an Al layer of 30 nm, a dead layer of 10 nm, a detector crystal thickness of 0.45 mm, a sample-to-detector distance of 57 mm, a detector area of 30 mm^2, 2000 channels each of 10 eV and a resolution of 124 eV (FWHM at Mn Kα). The detector elevation angle was set to 35°. An electron source with a Gaussian profile (5 nm Gaussian width) and in parallel illumination (zero beam divergence) was employed.

Geopolymer composites models

Two models were developed:

- The first one considers the case of a not completely reacted sodium-poly(sialate-siloxo) geopolymer (Na-PSS);
- The second one regards a geopolymer composite with a potassium-poly(sialate-siloxo) matrix (K-PSS) and basalt-derived glass fibres as reinforcement.

In details, in the first model a not completely reacted metakaolin particle (booklet), of composition $Si_2O_5Al_2O_2$, embedded in an "infinitely" extended Na-PSS matrix was simulated (Fig. 1a). Metakaolin is a very common starting raw material for geopolymer synthesis, and can be produced by a thermal dehydroxilation of natural kaolin, whose structural properties are also dependent on the microstrain [38]. The metakaolin particle was approximated with a rectangular cuboid 2 μm x 2 μm wide, with variable thickness (0.1, 0.3, 0.5, 0.75, 1, 3, 5, 7.5, 10 and 20 μm) and mass density of 2.4 g/cm^3 [39]. The simulated Na-PSS geopolymer presented a composition with oxides molar ratios Na_2O:Al_2O_3:$4SiO_2$:$6H_2O$, identified and selected as the typical stoichiometric composition of Na-PSS [2], and mass density of 1.45 g/cm^3 [2]. The energy of the electron beam, E_0, was varied between 2 and 20 keV (2, 3, 4, 5, 6, 7, 8, 9, 10, 15 and 20 keV) to study its effect on the analysis and find out the optimal working conditions, with the beam focussed in the middle of the particle upper surface.

The second simulated model is a fibre-reinforced geopolymer composite. A hemicylindrical basalt-derived glass fibre embedded in a K-PSS geopolymer matrix, "infinitely" thick compared to the depth of penetration of the electrons, was simulated to study the case of a fibre-reinforced geopolymer composite sectioned for SEM-EDS microanalysis (Fig. 1b). The radius of the fibre (in our model equal to the thickness of the hemicylinder) was varied between 0.1 and 20 μm (0.1, 0.3, 0.5, 0.75, 1, 3, 5, 7.5, 10 and 20 μm), with a fibre length of 50 μm, and investigating the effects of different electron beam energies, E_0: 5, 10, 15 and 20 keV. A characteristic composition of basalt-derived glass fibre (Table 1) was used [40–42], considering a mass density of 2.66 g/cm^3 [40,43,44]. The K-PSS geopolymer presented oxides molar ratios K_2O:Al_2O_3:$4SiO_2$:$6H_2O$, identified and selected as the typical stoichiometric composition of K-PSS [2], and mass density of 1.50 g/cm^3 [2]. The fibre long axis was oriented perpendicularly to the fibre-to-detector direction, with the electron beam placed on the centre of the fibre (Fig. 1b).

Results and discussion

SEM-EDS quantitative X-ray microanalysis relies on the assumption that the sample can be considered as a bulk material, defined as a material whose volume has a sufficiently large size to contain all the trajectories of the electrons and the generated X-rays. The microanalysis of composite materials with nano to microsized structures is therefore often a challenge. In these cases, large errors in the quantification could arise because of the extended scattering volume of the electrons with respect to the size of the investigated object, with not negligible effects, also influenced by shape-dependent factors. A good comprehension of complex physical phenomena that are at the basis of these issues can be achieved through a detailed SEM-EDS Monte Carlo investigation

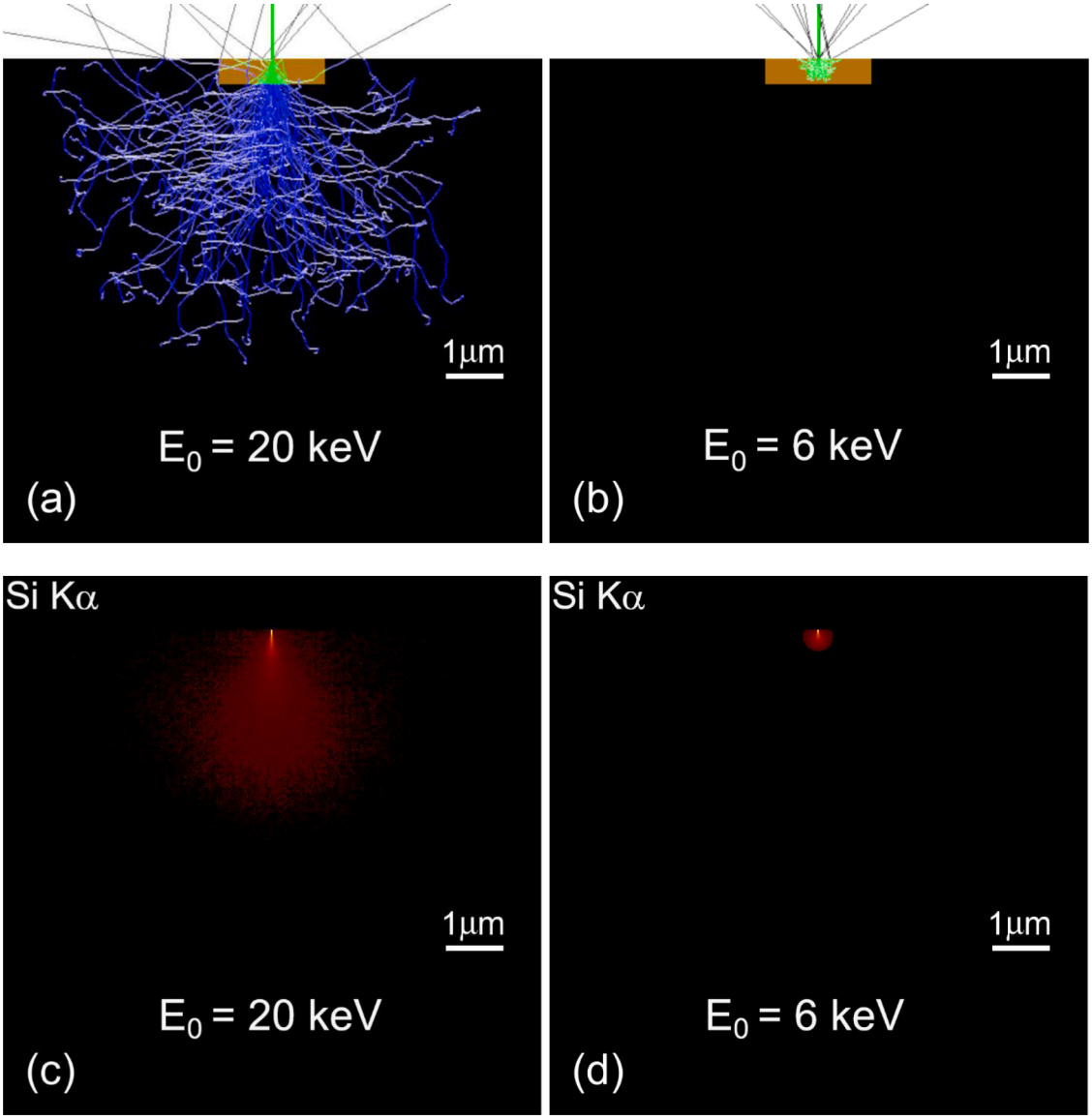

Fig. 2. (a,b) 2D projection of simulated 3D electron trajectories inside a metakaolin nanoparticle (brown area, 500 nm thick, and 2 μm wide) and Na-PSS geopolymer substrate (black area). Green and blue trajectories represent the electrons moving inside metakaolin and Na-PSS, respectively, whereas the grey ones are electrons escaping the sample surface. In panel (a) the electron beam energy is 20 keV, whereas in panel (b) it is 6 keV. (c,d) X-ray emission images of Si Kα line generated from the electron trajectories reported in (a) and (b), respectively.

[21–23].

As illustrated in the introduction, in the present work we simulated with Monte Carlo approach the SEM-EDS spectra of the two models, namely an unreacted metakaolin particle and a basalt-derived hemicylindrical glass fibre, both embedded in a specific geopolymer matrix. We considered realistic experimental conditions to obtain useful indications for a precise and accurate quantitative microanalysis of these two composite materials.

Unreacted metakaolin particle in Na-PSS geopolymer matrix

In an ideal geopolymerization reaction, it is expected that all the reagents (metakaolin, sodium silicate, etc.) transform into the desired geopolymer. However, the rate of reaction is not always 100% due to a variety of factor, such as, for example, the correct molar ratio between the reagents. Hence, it may be possible finding unreacted reagents embedded in the geopolymer matrix, by analysing the morphology and microchemistry of the geopolymerization products with SEM-EDS. Here, we modelled this kind of situation, considering a residual metakaolin nanoparticle, shaped as a simple prism with square base of 2 μm × 2 μm and a height between 100 nm and 20 μm, inside a Na-PSS geopolymer (Fig. 1a). The electron beam was focussed on the top of the particle in a centred position, and we investigated the effects of both the thickness of the prism and the energy of the electron beam (E_0 between 2 keV and 20 keV) on the microanalysis of the metakaolin nanoparticle.

To show how the choice of the acceleration voltage influences the SEM-EDS microanalysis, we report as an example the trajectories of electrons (Figs. 2a,b) and the X-ray emission image of Si Kα (Figs. 2c,d) obtained by focussing an electron beam with 20 keV and 6 keV energy on a metakaolin booklet 500 nm thick. Although the width of the electron beam is just 5 nm, when using high acceleration voltages (Fig. 2a) the electrons not only pass through the nanoparticle (green trajectories), travelling up to about 6 μm inside the geopolymer matrix (blue trajectories), but they are scattered laterally for more than 7 μm (blue trajectories). Hence, the volume of emission of X-rays extends well beyond the metakaolin volume, as reported for example for the Si Kα emission, which is mainly confined in a pear-like volume about 4 μm depth and about 3 μm wide (Fig. 2c). With these experimental settings, there is a

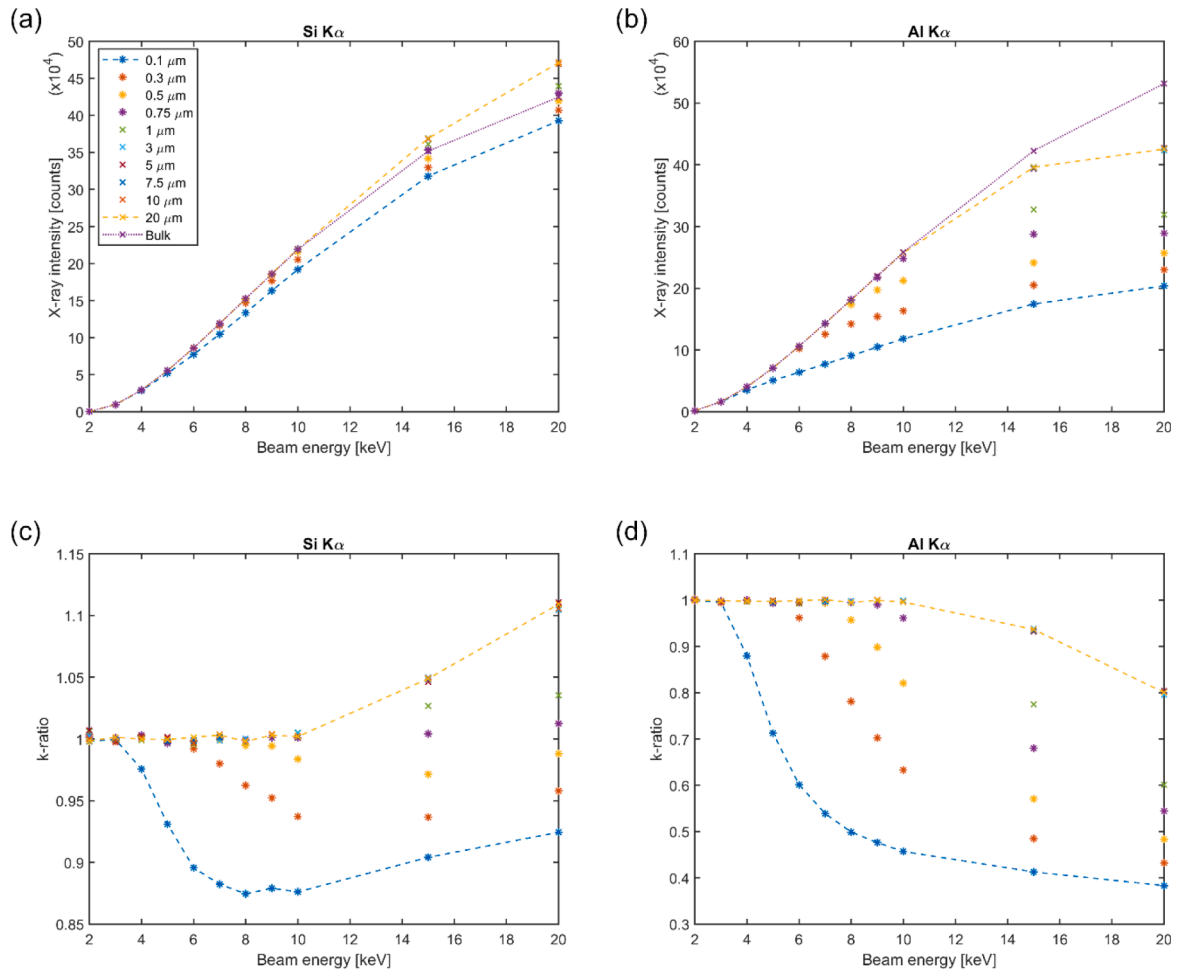

Fig. 3. Integrated X-ray intensities of (a) Si Kα line and (b) Al Kα line as a function of the electron beam energy, for different thicknesses of the metakaolin nanoparticle, including the trend simulated for the bulk-like material. Panels (c) and (d) report the k-ratios as a function of incident beam energy, calculated from the X-ray intensity data of the Si and Al Kα lines, respectively.

strong contribution of the geopolymer matrix to the SEM-EDS spectrum of the metakaolin nanoparticle, obviously leading to an erroneous analysis. The Monte Carlo simulation allowed to identify 6 keV as the optimal electron beam energy, because both the electron trajectories and X-ray emission volume are well confined inside the metakaolin nanoparticle. Hence, for an acceleration voltage of 6 kV, it is expected that a nanoparticle 500 nm thick behaves as a bulk of metakaolin, without any contribution from the surrounding matrix. This observation can also be extended to backscattered BS electrons (grey trajectories) that selectively come from the metakaolin particle surface when using a 6 keV beam, whereas even from the Na-PSS surface with a 20 keV beam (meaning a loss of BS signal from the investigated particle).

From the simulations, we obtained SEM-EDS spectra, as acquired from the specific silicon drift detector and SEM chamber setup here modelled, for the different particle thicknesses and electron beam energies. Secondary fluorescence generation and transport from Bremsstrahlung and primary characteristic X-rays were accounted for. Then, the background was removed and each characteristic X-ray line was integrated for each SEM-EDS spectrum.

The main results of the elaboration of the Monte Carlo data on the microanalysis of the embedded metakaolin nanoparticle are reported in Fig. 3. The first two panels (Fig. 3a,b) show the trend of the integrated X-ray intensity for the case of Si Kα X-ray line (1.740 keV) and Al Kα X-ray line (1.487 keV) as a function of the selected electron beam energy. The thickness of the metakaolin booklet was varied between 100 nm (dashed blue line with star marker) and 20 μm (dashed yellow line with x marker). Furthermore, we used the same SDD detector and SEM setup to perform a simulation of analysis on an "infinitely" extended metakaolin bulk sample chosen as reference standard and graphed the results as a dotted violet line with x marker. As shown in Fig. 3a,b a great variation of the X-ray intensity was observed depending on both the metakaolin thickness and specific beam energy, with Al Kα X-ray line, less energetic than Si Kα, presenting a more pronounced effect of intensity variation. To better evaluate and quantify the specific effects, we calculated the k-ratio, defined as the ratio between the integrated intensity calculated for a particular X-ray emission line of metakaolin (Mk) nanoparticle and the integrated intensity of the same X-ray line calculated for the bulk metakaolin (Fig. 3c,d). The desired optimal working conditions are therefore to be chosen between those operating conditions giving k-ratio close to 1. In the case of Si Kα X-ray line, as a general observation, a combination of $E_0 > 10$ keV and Mk thickness < 750 nm gives a loss of X-rays (k-ratio < 1), whereas $E_0 > 10$ keV and Mk thickness ≥ 750 nm gives an increase in X-rays (k-ratio > 1). The cause of this peculiar trend must be sought in the combination of elastic/inelastic scattering of electrons inside the booklet and Na-PSS geopolymer matrix, X-ray generation, transport, absorption and fluorescence, together with the booklet thickness and shape components (also taking into account the lateral size of 2 μm), silicon wt%, type of chemical elements and density of both metakaolin and geopolymer. For instance, focussing the attention on the use of a 15 keV beam, k-ratio < 1 for a thickness ≤ 500 nm due to the small mass of metakaolin excited by the electrons with respect to a bulk metakaolin. For thicknesses ≥ 1 μm, (i) an always higher percentage of

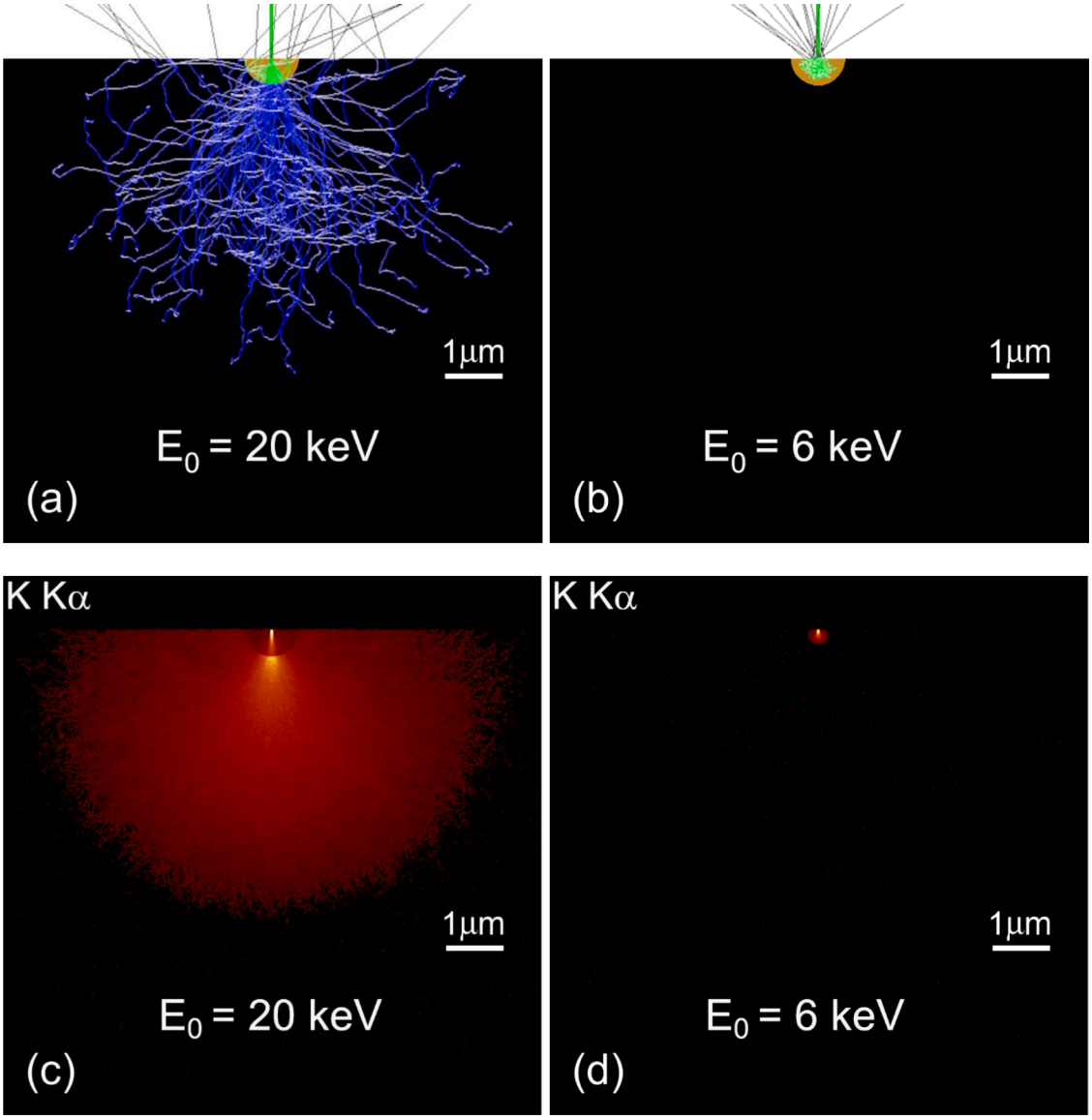

Fig. 4. (a,b) Simulated electron trajectories in the case of a basalt-derived glass fibre (brown area, radius of 500 nm) embedded in a K-PSS geopolymer matrix (black area). Green and blue trajectories represent the electrons moving inside metakaolin and K-PSS geopolymer, respectively, whereas the backscattered electrons are represented by grey lines. In panel (a) the electron beam energy is 20 keV, whereas in panel (b) it is 6 keV. (c,d) X-ray emission images of K Kα line generated from the electron trajectories reported in (a) and (b), respectively.

the detected Si Kα X-rays is generated inside metakaolin, and (ii) these X-rays undergo a reduced absorption with respect to a bulk metakaolin, because of the lower mean atomic number and density of the geopolymer matrix. The case of the 750 nm thick booklet is a very particular condition, where the combination of X-ray generation and absorption gives a k-ratio near to the bulk case. On the contrary, focussing the attention on the use of a 10 keV beam, the lateral extension of the detected Si Kα X-rays is about only 1.2 μm (well below the metakaolin lateral size of 2 μm; data not showed) and thus the above cited reduced absorption effect is minimized, with k-ratio ≤ 1.

Independently on E_0 and Mk thickness, for $E_0 \leq 10$ keV and Mk thickness ≥ 750 nm Si Kα X-rays are comparable with a Mk bulk (k-ratio ~ 1). Differently, Al Kα X-ray line has a bulk-like behaviour (k-ratio ~ 1) for $E_0 \leq 10$ keV and Mk thickness ≥ 1 μm, independently on E_0 and Mk thickness, whereas a strong X-ray reduction is observed particularly for high E_0 and/or low thickness, up to more than 60% in the case of $E_0 = 20$ keV and Mk thickness of 20 μm.

The curves of k-ratio suggest the optimal working energy (i.e., where k-ratio ~ 1) for each specific thickness, being a compromise between the deviation from the bulk counts and the necessity of achieving high X-ray counts for statistical reasons.

Basalt-derived glass fibre-reinforced K-PSS geopolymer composite

The second case of geopolymer composite was a 3D hemicylindrical basalt-derived glass fibre, of composition reported in Table 1, embedded in a K-PSS geopolymer matrix, representing an example of sample specifically sectioned and polished for SEM-EDS X-ray microanalysis (Fig. 1b). To study the effects of the sample geometry and of the chosen electron beam energy E_0 on the X-ray microanalysis and to identify the optimal working settings that should be used to avoid quantification errors, the radius of the hemicylindrical fibre, here also representing its maximum thickness, was varied between 100 nm and 20 μm, and at the same time the beam energy was varied between 5 keV and 20 keV.

Figs. 4a,b show two examples of electron trajectory images generated by the Monte Carlo simulations. They represent a 2D projection (x-z plane) of the 3D electron trajectories inside a fibre with radius of 500 nm (coloured in brown) and the surrounding K-PSS matrix (coloured in

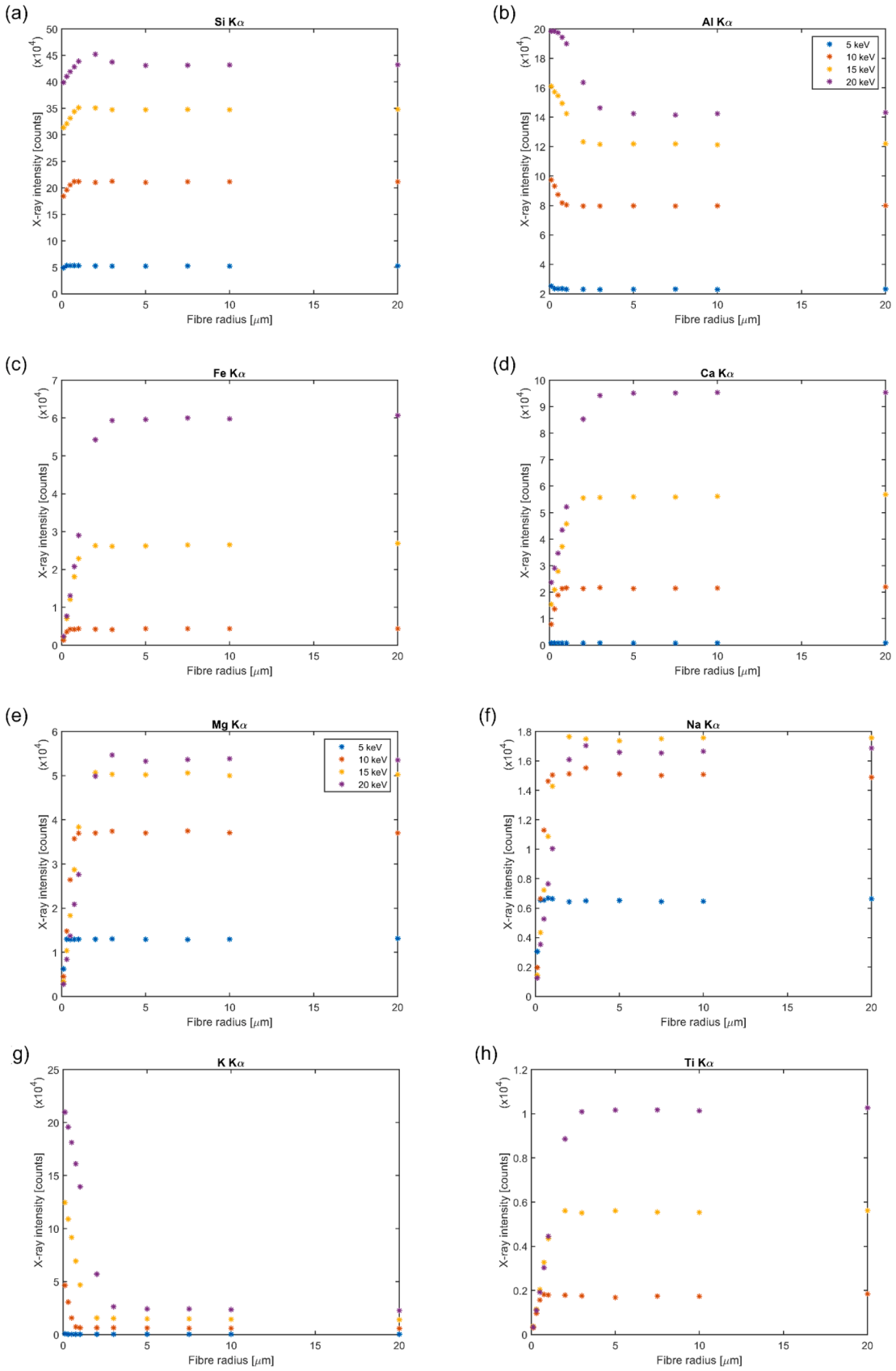

Fig. 5. Integrated X-ray intensities for the Kα lines of (a) Si, (b) Al, (c) Fe, (d) Ca, (e) Mg, (f) Na, (g) K and (h) Ti, as a function of the electron beam energy. Different radii of the hemicylindrical fibre were considered, between 100 nm and 20 μm. Legend in (b).

black). Notwithstanding the ideal focussing of the electron beam in the middle of the fibre and the use of an electron probe of just 5 nm in width (green vertical beam), a typical acceleration voltage of 20 kV allows electrons to pass through the fibre (green trajectories) and penetrate the geopolymer matrix (blue trajectories) for up to about 6 μm in depth and laterally scattering for about 8 μm (Fig. 4a). The resulting SEM-EDS spectrum will necessarily be a combination of X-rays from the fibre and form the matrix, with a great contribution from the latter (data not shown). As an example, Fig. 4c reports the X-ray emission image of K Kα line generated by the electron trajectories of Fig. 4a, evidencing an X-ray distribution close to the electron trajectories' one, widely produced inside the geopolymer matrix. By investigating the various configurations through Monte Carlo simulation, it was determined that the use of an electron beam of 6 keV, at the specific conditions taken into account in our model and for a fibre with a radius of 500 nm, strictly confines the electron trajectories (Fig. 4b) and also the X-ray generation volume (see Fig. 4d for the case of K Kα line) inside the fibre. In this last case, even the backscattered electrons (grey trajectories) only escape from the fibre.

In general, the trend of the integrated X-ray intensities as a function of the hemicylindrical fibre radius showed a pronounced non-linear reduction at the lowest thicknesses in the case of Si Kα, Fe Kα, Ca Kα, Mg Kα, Na Kα, Ti Kα, whereas an X-ray increase for Al Kα and K Kα (because of the contribution from the Al and K rich geopolymer matrix), with peculiar trends for each beam energy and type of X-ray line investigated. In particular, the variations in intensity were observed for radii of the hemifibre lower than 3 μm at 20 keV, 2 μm at 15 keV, 1 μm at 10 keV and 0.3 μm at 5 keV, meaning that below these thickness values the X-ray generation volume is greater than the fibre radius.

Fig. 5 shows the results of the integration of X-ray peaks from the simulated EDS spectra for Si Kα, Al Kα, Fe Kα, Ca Kα, Mg Kα, Na Kα, K Kα and Ti Kα, reported as a function of the basalt-derived fibre radius for the considered beam energies of 5 keV (blue), 10 keV (red), 15 keV (yellow) and 20 keV (violet). Decreasing the fibre radius, Si Kα (1.740 keV) presented a peculiar trend with an initial increase of the integrated intensity below 5 μm, more accentuated at 20 keV, followed by a fast decrease below 2 μm. It means that, at 20 keV, the measurement of Si Kα X-rays from the fibre would be correct for a radius higher than about 5 μm, whereas it will be overestimated for a radius between about 5 and 1 μm, and underestimated for a radius lower than about 1 μm. This behaviour can be explained with a prevalence of the reduced X-ray absorption effect over the finite size (mass) one for 1 μm $\leq$ radius $<$ 5 μm. It should be noted that an electron beam of 5 keV is not enough energetic to induce Fe Kα and Ti Kα X-ray generation, due to the high K absorption edges of 7.112 keV and 4.967 keV, respectively. Similarly, Ca and K atoms are not efficiently excited by a beam of 5 keV, being this energy close to the respective K absorption edges, 4.038 keV and 3.607 keV.

It is thus clear that a researcher interested in performing a quantitative SEM-EDS X-ray microanalysis of a basalt-derived glass fibre, employing the experimental conditions modelled in the present work, would make substantial errors, if he did not carefully consider the measurement issues here highlighted. For instance, for a fibre with a radius of 500 nm analysed with a 15 keV beam, an underestimation of about 5 % for Si Kα, 45 % for Fe Kα, 50 % for Ca Kα, 35 % for Mg Kα, 40 % for Na Kα, 35 % for Ti Kα, and an overestimation of about 25 % for Al Kα and even 650 % for K Kα, would be obtained.

Conclusions

The present work highlighted that SEM-EDS qualitative and quantitative X-ray microanalysis of geopolymer composite materials should be carefully designed in order to avoid possible errors or misinterpretations. The SEM-EDS Monte Carlo approach was demonstrated to be an effective strategy to predict the several potential issues associated with the investigation of the nano-micro sized architecture of the composite geopolymers. The specific geometry (thickness and shape), features, chemistry and electron beam energy could play an important role in the precision and accuracy of the analysis. Other particular conditions easily faced during a routine analysis, like for instance a not ideally centred beam, a fibre not perfectly straight, or uniform in radius, are expected to further affect the measurement. Errors up to several tens of percentages in the X-ray intensity measurement were calculated from the models and specific SEM-EDS set-up here simulated. However, it was also demonstrated that the Monte Carlo approach can determine the optimal SEM-EDS instrumental parameters that should be employed for each specific sample arrangement in order to perform a precise and accurate qualitative and quantitative analysis.

Declaration of interests

The authors declare that they have no known competing financial interests or personal relationships that could have appeared to influence the work reported in this paper.

References

[1] J. Davidovits, Polymère Minéral (1979). FR2464227A1.
[2] J. Davidovits, Geopolymer Chemistry and Applications, Institut Géopolymère, 2020, 5th ed. Saint-Quentin, France.
[3] G Ulian, G. Valdrè, Density functional investigation of the thermophysical and thermochemical properties of talc [Mg3Si4O10(OH)2], Phys. Chem. Miner. 42 (2015) 151–162, https://doi.org/10.1007/S00269-014-0708-7.
[4] G Ulian, G Valdrè, M Corno, P. Ugliengo, DFT investigation of structural and vibrational properties of type B and mixed A-B carbonated hydroxylapatite, Am. Mineral. 99 (2014) 117–127, https://doi.org/10.2138/AM.2014.4542.
[5] P Duxson, JL Provis, GC Lukey, SW Mallicoat, WM Kriven, JSJ. Van Deventer, Understanding the relationship between geopolymer composition, microstructure and mechanical properties, Colloids Surf A Physicochem Eng Asp 269 (2005) 47–58, https://doi.org/10.1016/J.COLSURFA.2005.06.060.
[6] P Duxson, A Fernández-Jiménez, JL Provis, GC Lukey, A Palomo, JSJ. van Deventer, Geopolymer technology: the current state of the art, J. Mater. Sci. 42 (2007) 2917–2933, https://doi.org/10.1007/S10853-006-0637-Z.
[7] I Giannopoulou, D. Panias, Hydrolytic stability of sodium silicate gels in the presence of aluminum, J. Mater. Sci. 45 (2010) 5370–5377, https://doi.org/10.1007/S10853-010-4586-1.
[8] D Moro, G Ulian, G. Valdrè, Nanoscale cross-correlated AFM, Kelvin probe, elastic modulus and quantum mechanics investigation of clay mineral surfaces: The case of chlorite, Appl. Clay Sci. 131 (2016) 175–181, https://doi.org/10.1016/J.CLAY.2015.11.023.
[9] A Gatti, G Valdre, A. Tombesi, Importance of microanalysis in understanding mechanism of transformation in active glassy biomaterials, J. Biomed. Mater. Res. 31 (1996) 475–480.
[10] G Valdrè, GA Botton, LM. Brown, High spatial resolution PEELS characterization of FeAl nanograins prepared by mechanical alloying, Acta Mater. 47 (1999) 2303–2311, https://doi.org/10.1016/S1359-6454(99)00066-X.
[11] GC Borgia, RJS Brown, P Fantazzini, E Mesini, G. Valdre, Diffusion-weighted spatial information from 1 H relaxation in restricted geometries, Nuovo Cim D 14 (1992) 745–759, https://doi.org/10.1007/BF02451721.
[12] T Lin, D Jia, P He, M. Wang, In situ crack growth observation and fracture behavior of short carbon fiber reinforced geopolymer matrix composites, Mater Sci Eng A 527 (2010) 2404–2407, https://doi.org/10.1016/J.MSEA.2009.12.004.
[13] IM Low, editor. Advances in Ceramic Matrix Composites, Elsevier, 2018, https://doi.org/10.1016/C2016-0-03477-0, 2nd ed. Duxford, UK.
[14] E Monaldo, F Nerilli, G. Vairo, Basalt-based fiber-reinforced materials and structural applications in civil engineering, Compos. Struct. 214 (2019) 246–263, https://doi.org/10.1016/J.COMPSTRUCT.2019.02.002.
[15] V Fiore, T Scalici, G Di Bella, A. Valenza, A review on basalt fibre and its composites, Compos. Part B Eng. 74 (2015) 74–94, https://doi.org/10.1016/J.COMPOSITESB.2014.12.034.
[16] AT Akono, S Koric, WM. Kriven, Influence of pore structure on the strength behavior of particle- and fiber-reinforced metakaolin-based geopolymer composites, Cem. Concr. Compos. 104 (2019), 103361, https://doi.org/10.1016/J.CEMCONCOMP.2019.103361.
[17] M Frydrych, Hýsek Š, L Fridrichová, Herclík M Van S Le, M Pechočiaková, et al., Impact of Flax and Basalt Fibre Reinforcement on Selected Properties of Geopolymer Composites, Sustainability 12 (2019) 118, https://doi.org/10.3390/SU12010118.
[18] Z Guo, C Wan, M Xu, J. Chen, Review of Basalt Fiber-Reinforced Concrete in China: Alkali Resistance of Fibers and Static Mechanical Properties of Composites, Adv. Mater. Sci. Eng. (2018), 9198656, https://doi.org/10.1155/2018/9198656.
[19] NWM. Ritchie, Using DTSA-II to Simulate and Interpret Energy Dispersive Spectra from Particles, Microsc. Microanal. 16 (2010) 248–258, https://doi.org/10.1017/S1431927610000243.
[20] NWM. Ritchie, Efficient Simulation of Secondary Fluorescence Via NIST DTSA-II Monte Carlo, Microsc. Microanal. 23 (2017) 618–633, https://doi.org/10.1017/S1431927617000307.

[21] G Valdrè, D Moro, G. Ulian, Monte Carlo simulation of the effect of shape and thickness on SEM-EDS microanalysis of asbestos fibres and bundles: the case of anthophyllite, tremolite and actinolite, IOP Conf. Ser. Mater. Sci. Eng. 304 (2018), 012019, https://doi.org/10.1088/1757-899X/304/1/012019.
[22] D Moro, G Ulian, G. Valdrè, Monte Carlo SEM-EDS micro- and nanoanalysis of ultrathin gold leaves in glass mosaic tesserae: Thickness effects and measurement strategy, Measurement 129 (2018) 211–217, https://doi.org/10.1016/J.MEASUREMENT.2018.07.025.
[23] D Moro, G Ulian, G. Valdrè, SEM-EDS microanalysis of ultrathin glass and metal fragments: measurement strategy by Monte Carlo simulation in Cultural Heritage and Archaeology, Int. J. Conserv. Sci. 11 (2020) 223–232.
[24] NWM. Ritchie, Spectrum Simulation in DTSA-II, Microsc. Microanal. 15 (2009) 454–468, https://doi.org/10.1017/S1431927609990407.
[25] R Myklebust, D Newbury, H Yakowitz. NBS Monte Carlo Electron Trajectory Calculation Program, Special Ed. Whashington: National Bureau of Standards, 1976, https://doi.org/10.6028/NBS.SP.460.
[26] Z Czyżewski, DO MacCallum, A Romig, DC. Joy, Calculations of Mott scattering cross section, J. Appl. Phys. 68 (1990) 3066, https://doi.org/10.1063/1.346400.
[27] A Jablonski, F Salvat, CJ Powell, NIST electron elastic-scattering cross-section, database (2010).
[28] DC Joy, S. Luo, An empirical stopping power relationship for low-energy electrons, Scanning 11 (1989) 176–180, https://doi.org/10.1002/SCA.4950110404.
[29] HA Bethe, J. Ashkin, Passage of radiation through matter, In: Segre E, editor. Exp, Nucl. Phys. (1953). New York, N.Y.: John Wiley & Sons.
[30] D Bote, F. Salvat, Calculations of inner-shell ionization by electron impact with the distorted-wave and plane-wave Born approximations, Phys. Rev. A 77 (2008), 042701, https://doi.org/10.1103/PhysRevA.77.042701.
[31] D Bote, F Salvat, A Jablonski, CJ. PowellCross sections for ionization of K, M L, shells of atoms by impact of electrons and positrons with energies up to 1 GeV: Analytical formulas, At. Data Nucl. Data Tables 95 (2009) 871–909, https://doi.org/10.1016/J.ADT.2009.08.001.
[32] ST Perkins, DE Cullen, MH Chen, J Rathkopf, J Scofield, JH. Hubbell, Tables and graphs of atomic subshell and relaxation data derived from the LLNL Evaluated Atomic Data Library (EADL), Z = 1–100, Lawrence Livermore National Laboratory, Berkley, CA, 1991, https://doi.org/10.2172/10121422.
[33] E Acosta, X Llovet, F. Salvat, Monte Carlo simulation of bremsstrahlung emission by electrons, Appl. Phys. Lett. 80 (2002) 3228, https://doi.org/10.1063/1.1473684.
[34] F Salvat, JM Fernandez-Varea, Sempau J. PENELOPE, A code system for Monte Carlo simulation of electron and photon transport, OECD, 2014, https://doi.org/10.1787/4E3F14DB-EN. Issy-Les-Moulineaux, France2015.
[35] SM Seltzer, MJ. Berger, Bremsstrahlung spectra from electron interactions with screened atomic nuclei and orbital electrons, Nucl Instruments Methods Phys. Res. Sect. B Beam Interact with Mater Atoms 12 (1985) 95–134, https://doi.org/10.1016/0168-583X(85)90707-4.
[36] SM Seltzer, MJ. Berger, Bremsstrahlung energy spectra from electrons with kinetic energy 1 keV–10 GeV incident on screened nuclei and orbital electrons of neutral atoms with Z = 1–100, At. Data Nucl. Data Tables 35 (1986) 345–418, https://doi.org/10.1016/0092-640X(86)90014-8.
[37] CT Chantler, K Olsen, RA Dragoset, J Chang, AR Kishore, SA Kotochigova, et al., X-Ray Form Factor, Attenuation, Scattering Tables (2005) version 2.1.
[38] F Dellisanti, G. Valdrè, The role of microstrain on the thermostructural behaviour of industrial kaolin deformed by ball milling at low mechanical load, Int. J. Miner. Process. (2012) 69–77, https://doi.org/10.1016/J.MINPRO.2011.09.011, 102–103.
[39] A Gualtieri, M. Bellotto, Modelling the structure of the metastable phases in the reaction sequence kaolinite-mullite by X-ray scattering experiments, Phys. Chem. Miner. 25 (1998) 442–452, https://doi.org/10.1007/S002690050134.
[40] YV. Lipatov, SI Gutnikov, MS Manylov, ES Zhukovskaya, BI. Lazoryak, High alkali-resistant basalt fiber for reinforcing concrete, Mater. Des. 73 (2015) 60–66, https://doi.org/10.1016/J.MATDES.2015.02.022.
[41] C Tang, H Jiang, X Zhang, G Li, J. Cui, Corrosion Behavior and Mechanism of Basalt Fibers in Sodium Hydroxide Solution, Materials (Basel) 11 (2018) 1381, https://doi.org/10.3390/MA11081381.
[42] V Pastsuk, M Kiisk, R Lõhmus, M Merisalu, S Kovaljov, A Biland, et al., Selection of basalt fiber with resistance to concrete alkaline environment, SN Appl. Sci. 2 (2020) 1–17, https://doi.org/10.1007/S42452-020-03677-Z.
[43] J Sim, C Park, DY. Moon, Characteristics of basalt fiber as a strengthening material for concrete structures, Compos. Part B Eng. 36 (2005) 504–512, https://doi.org/10.1016/J.COMPOSITESB.2005.02.002.
[44] W Li, J Xu, Mechanical properties of basalt fiber reinforced geopolymeric concrete under impact loading, Mater. Sci. Eng. A 505 (2009) 178–186, https://doi.org/10.1016/J.MSEA.2008.11.063.